Coherent phase stability in Al-Zn and Al-Cu fcc alloys: The role of the instability of fcc Zn

S. Müller, L.-W. Wang, and Alex Zunger
National Renewable Energy Laboratory, Golden, Colorado 80401

C. Wolverton
Ford Research Laboratory, MD3028/SRL, Dearborn, Michigan 48121-2053

(Received 29 July 1999)

The coherent phase stability of fcc-based Al-Zn and Al-Cu alloys is studied theoretically by first-principles total energy calculations, a mixed-space cluster expansion approach, and Monte Carlo thermodynamic simulations. We find that a large portion of the differences between Al-Zn and Al-Cu can be explained by the differences between fcc-Zn and fcc-Cu: While Zn is stable in the hcp structure, fcc-Zn shows an instability when deformed rhombohedrally along (111). In contrast, fcc-Cu is the stable form of Cu and is elastically extremely soft when deformed along (100). These elastically soft directions of the constituents permeate the phase stability of the alloys: (111) superlattices are the lowest energy coherent structures in Al-Zn, while (100) superlattices are stable coherent phases in Al-Cu. The short-range order of both Al-rich solid solutions show clustering tendencies, with the diffuse intensity due to short-range order in Al-Zn and Al-Cu showing streaks along (111) and (100), respectively. The mixing enthalpies and coherent phase boundaries are also calculated and found to be in good agreement with experimental data, where available. [S0163-1829(99)01146-7]

I. INTRODUCTION

Al_xZn_{1-x} and Al_xCu_{1-x} alloys, generally with other additions, form two important families of commercial aluminum alloys (see, e.g., Ref. 1, and references therein). Remarkably, the phase diagrams and thermodynamic properties of the binary systems differ profoundly even though Cu and Zn are nearest neighbors in the periodic table: Al_xZn_{1-x} is a phase-separating system with *positive* mixing enthalpy exhibiting a wide fcc miscibility gap in the phase diagram and clustering-type short-range order in diffuse scattering experiments.[2,3] The miscibility gap in Al-Zn has made this system a prototype for studies of spinodal decomposition in alloys (e.g., see Refs. 4–6 and Ref. 7). In contrast, Al_xCu_{1-x} is a compound-forming system with *negative* mixing enthalpy showing many intermediate ordered phases in its phase diagram and exhibiting short-range order in diffuse scattering experiments of clustering-type for Al-rich compositions[8] and ordering-type for Cu-rich compositions.[9–12] While Al_xZn_{1-x} exhibits solid solutions over large temperature and composition regimes (in fact, Zn has the largest solubility in Al of any element in the periodic table[1]), the solid solution regime in the phase diagram of Al_xCu_{1-x} is limited to compositions of about 2% Cu.[13–15]

In this paper, we analyze theoretically the phase stability and ordering tendencies of these two alloy systems. We use the first-principles mixed space cluster expansion[16,17] in which the $T=0$ total energies of a few ordered A_pB_q compounds are computed via the local density approximation (LDA) and used to construct a generalized Ising-like expansion that describes the configurational energy of the alloy via pair and multibody effective cluster interaction energies. The total energies which are needed as input for the cluster expansion were calculated using the pseudopotential method for Al-Zn and the full-potential linearized augmented plane wave method (LAPW) for Al-Cu (details are provided in the Appendix). The cluster expansion is then subjected to Monte Carlo simulations that produce both $T=0$ ground states and thermodynamic properties such as coherent composition-temperature phase boundaries, mixing enthalpies, and atomic short-range order of the solid solution, all of which are compared with experiment. We show how the different physical properties of the Al_xZn_{1-x} vs Al_xCu_{1-x} alloys to a large extent reflect the difference in stability of fcc-Zn vs fcc-Cu.

Our study leads to a surprising result: First principles total energy calculations indicate an *instability of elemental fcc-Zn when distorted rhombohedrally along (111)* [or orthorhombically along (110)]. This instability has profound consequences for the phase stability of fcc Al_xZn_{1-x} alloys: Strain energies and formation enthalpies of Al_pZn_q (111) superlattices become unusually low. While (100) represents the elastically softest direction in (Al-rich) Al-Cu and (111) the elastically hardest direction, in Al-Zn the order is reversed—(100) is hardest and (111) softest. Therefore, finite temperature studies of Al-rich alloys find short-range order at (000) with streaks along the (100) direction for Al-Cu, but along (111) for Al-Zn.

One characteristic which Al_xZn_{1-x} and Al_xCu_{1-x} alloys share is that both are heat treatable, i.e., both alloys can be hardened or strengthened by controlled heating and cooling. The increased hardness of the alloys is due to the formation of precipitates which act as obstacles for dislocation motion. Knowledge of the shapes and sizes of the precipitates is essential towards understanding the strengthening mechanisms in these alloys. A prerequisite for a detailed study of precipitate shapes is the knowledge of the *coherent phase boundaries*, i.e., the locus of composition-temperature points at which solubility in the solid solution phase is lost and coherent precipitation (i.e., with no dislocations between precipitate and matrix) occurs. The coherent miscibility gap in Al-Zn alloys is therefore of great interest and has been studied using a wealth of experimental techniques (see Ref. 7 for an assessment of the experimental data). The coherent phase boundary is depressed below the equilibrium incoherent miscibility gap due to the elastic strain associated with maintaining coherency between precipitate and matrix.[4,5] Experimental measurements of the top of the coherent miscibility gap from direct measurement techniques, such as x-ray diffrac-

tion, TEM studies, and neutron scattering studies[18–20] give values from 318–328 °C for compositions of about 37–40 % Zn. (Assessing the coherent phase boundary via aging at low temperatures and reheating to find the reversion temperature is problematic due to the complex precipitation kinetics at low temperatures.[7]) Decomposition of the solid solution at temperatures below the coherent phase boundary gives rise to a series of coherent fcc precipitate shapes. The precipitation sequence involves spherical Guinier-Preston (GP) zones,[7,21] coherent ellipsoidal precipitates, and partially coherent platelets [with coherency along (111)].[22–26]

The decomposition of Al-rich Al_xCu_{1-x} solid solutions also produces coherent GP zones. In fact, Al-Cu alloys provide the textbook example of the formation of GP zones in supersaturated solid solutions.[27,28,21] The specifics of the precipitation sequence are somewhat controversial, but it is generally agreed that coherent platelets of Cu form along (100) directions.[28] Two types of GP zones have been reported, the so-called GP1 and GP2 zones.[28] There have been many measurements of the coherent phase boundaries for GP1 and GP2 zones (see Ref. 75, and references therein) which show a maximum temperature of roughly 200 °C at the solubility limit of 2% Cu. Recently, the mixed-space cluster expansion technique used here has been applied to Al-Cu alloys and the resulting coherent phase boundaries and precipitates predicted.[29] This theoretical approach was shown to provide predictions for the coherent precipitate shapes of GP1 and GP2, and also provides an explanation for the GP1-GP2 transition observed in terms of a size-dependent transition of the equilibrium precipitate shape.

Here, we construct a mixed-space cluster expansion for Al-Zn alloys using first-principles total energy calculations. Then, we compare the resulting phase stability of Al-Zn with the previous calculations of Al-Cu (Ref. 29) in terms of their zero-temperature superlattice energies and ground states, as well as thermodynamic properties such as mixing enthalpies, coherent phase boundaries, and short-range order in the solid solutions. We show how the instability of fcc-Zn is, to a large extent, responsible for many of the thermodynamic properties of Al-Zn, and is hence responsible for the contrast between many properties of Al-Zn and Al-Cu. All of these results are compared with experimental observations, where available. The calculations described here create a basis for a detailed theoretical study of precipitation in Al-Zn.

II. INSTABILITY OF ELEMENTAL FCC ZN

The constituents of the two considered alloys Cu, Al, and Zn, have different structural preferences: while Cu and Al crystallize in an fcc lattice, Zn is hcp. Confronted with the problem of describing the fcc solid solution in the Al_xZn_{1-x} alloy system we have to inquire about the stability and elastic properties of this unusual phase: fcc-Zn. Figure 1 compares LDA-calculated total energies of volume-conserving distortions along the three principal crystallographic directions for fcc-Cu (a) and fcc-Zn (b). The calculation is volume conserving in that the ''basal plane'' lattice constants a are varied, while the third lattice constant c is chosen so as to maintain the constant volume of the undistorted unit cell. We define $c/a=1$ as the undistorted fcc state. We used the pseudopotential method, as detailed in the Appendix. Figure

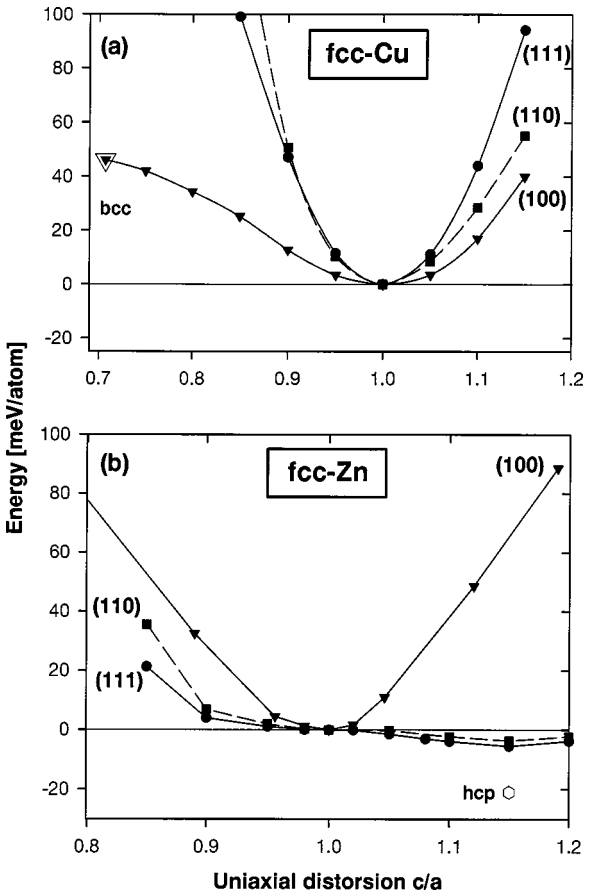

FIG. 1. Volume-conserving first-principles total energy calculations of (a) fcc-Cu and (b) fcc-Zn deformed along different crystallographic directions. The energy differences caused by distortions along (100), (110), and (111) as well as for bcc Cu and hcp Zn are always given with respect to the undistorted fcc lattice. The energy of bcc Cu is denoted as an open triangle, while the energy of hcp Zn is denoted as an open hexagon.

1 demonstrates that Cu has a minimum energy at the undistorted ($c/a=1$) fcc structure (as it must, since fcc is the stable form of Cu), while the bcc structure ($c/a=1/\sqrt{2}$) is 46 meV/atom higher in excellent agreement with earlier LAPW studies.[30] In contrast, the stable hcp form of Zn is 21 meV/atom lower in energy than fcc Zn. Furthermore, while all the energies of ''distorted'' fcc-Cu show the expected parabolic shape exhibiting a minimum for the undistorted fcc structure, distorting fcc-Zn produces an intriguing result: The volume conserving total energies for fcc-Zn [Fig. 1(b)] show *an instability of fcc-Zn when rhombohedrally distorted along (111) or orthorhombically distorted along (110).* Total energy minima occur at $c/a\approx 1.15$ lying -5.5 and -3.7 meV below the energy level of the ideal undistorted fcc-Zn unit cell for (111) and (110), respectively. This instability is, as we show below, essential for a correct description of the properties of Al-Zn alloys. Because of their central role in this work the curves of Fig. 1 were also calculated using the LAPW method. The agreement between pseudopotential and LAPW total energies is excellent: Deviations are smaller than 3 meV for each individual c/a ratio, and the LAPW results show the same instability of fcc Zn with respect to (111) and (110) distortions at $c/a\approx 1.15$.

The instability of elemental metals in crystal structures other than their stable state has been found (theoretically)

many times before.[31–35] However, the most common example is fcc-stable elements (e.g., Cu) which are unstable in the bcc structure, or vice versa. [The 100-type distortion connects the fcc and bcc structures via the Bain path, and the instability of bcc Cu can be seen from the 100 distortion in Fig. 1(a).] This fcc-bcc instability may be phrased in terms of elastic constants by a negative value of $C_{11}-C_{12}$ for the unstable phase. However, the instability in fcc Zn is due to a negative value of C_{44} and is, to the authors' knowledge, the first known case of an hcp element which is unstable in the fcc structure. Furthermore, as we show below, the instability of fcc-Zn permeates the energetics of fcc-based Al-Zn alloys and effects strain energetics, ordered formation enthalpies, and thermodynamic properties such as the atomic short-range order. The instability of fcc Zn is also expected to have consequences in the stacking fault energies in hcp Zn and also in any experiments which might attempt to epitaxially grow a stable form of fcc Zn.

The c/a ratio (with respect to ideal close packing) at which the fcc-Zn total energy has a minimum is practically identical to the c/a ratio in hcp Zn [shown in Fig. 1(b) as a hexagon]. Experimentally, hcp Zn has an anomalously large c/a ratio of 1.15 (with respect to ideal close packing). A study by Singh and Papaconstantopoulos[36] shows that the density of states of hcp Zn for $c/a=1.15$ shows a splitting of states, which leads to a low density of states at the Fermi level. In contrast, at the ideal c/a the density of states at the Fermi level is even larger than that calculated for undistorted fcc Zn. The authors suggest that this change in the density of states is responsible for the anomalous c/a ratio in hcp Zn and that the Zn d states play an important role in the stability of hcp Zn. A recent paper reaches a similar conclusion: Zheng-Johansson, Eriksson, and Johansson[37] show that the deviation of c/a in hcp Zn is caused by the one electron d-band energy and therefore to the d-band filling. This work shows that the Madelung energy and, to lesser extent, the Born-Mayer repulsion stabilize the hcp crystal at the ideal axial ratio, while the one-electron d-eigenvalue sum having a distorted asymmetric parabolic c/a dependence is the dominant term that favors a deviation of the axial c/a ratio from the ideal one. The observation of the large c/a instability in fcc-Zn [Fig. 1(b)] suggests that the physical mechanism which is responsible for the anomalous c/a ratio of hcp-Zn could be the same as that which causes the instability of fcc Zn. Indeed, the development of an energy minimum of fcc Zn at the same c/a ratio as stable hcp Zn is indicative of the propensity of the former to ''imitate'' the latter.

III. AL-ZN VERSUS AL-CU: COMPARISON OF ALLOY STRAIN ENERGIES AND FORMATION ENTHALPIES

We next investigate the consequences of the instability of fcc Zn on the properties of fcc Al_xZn_{1-x} alloys. We will thus compute the strain energies of Al_xZn_{1-x} and Al_xCu_{1-x} alloys and show how the behavior (Fig. 1) of the elements Cu and Zn effect the alloy properties.

A. Elemental epitaxial energies

A description of the strain properties of alloys requires specifying two types of quantities[38]

(a) The *hydrostatic deformation energy* $\Delta E_A^{\text{bulk}}(a)$ which is the energy required to hydrostatically deform the solid element A to the lattice constant a of the alloy.

(b) The *epitaxial strain energy* $\Delta E_A^{\text{epi}}(a,\hat{G})$, representing the energy of the elemental solid A epitaxially (or, biaxially) deformed to the ''substrate'' lattice constant a in the two directions orthogonal to $\hat{G}$ and *relaxed* along $\hat{G}$.

Thereby, it is important to mention that all energy differences in this work are given with respect to the ideal *undistorted* fcc structure of Cu, Al, and Zn. The ratio of the two energies given above defines the *epitaxial softening function*[38,39]

$$q(a,\hat{G})=\frac{\Delta E_A^{\text{epi}}(a,\hat{G})}{\Delta E_A^{\text{bulk}}(a)}. \tag{1}$$

Since it is always easier to deform a material epitaxially (biaxially) than hydrostatically (triaxially), $q\leqslant 1$. Small values of $q(\hat{G})$ indicate elastically soft directions $\hat{G}$. The difference between ΔE^{epi} and the volume-conserving calculations of Fig. 1 is that the lattice vector along $\hat{G}$ is relaxed in the epitaxial calculations, while in a volume-conserving calculation it is fixed by the constant-volume condition.

In the harmonic elasticity theory, q depends only on the direction $\hat{G}$, but not on the substrate lattice constant a.[38,16,40] Recent studies have demonstrated that anharmonic effects can be important and therefore, q becomes a function of the substrate lattice parameter a.[42,43] Figure 2 shows our LDA-calculated epitaxial softening ratio $q(a,\hat{G})$. The shaded areas denote the lattice parameter range pertinent to the alloys studied. We note the following: (i) Zn shows overall the smallest q values, i.e., relative to hydrostatic deformation, epitaxially deformed Zn is softer than Cu or Al. (ii) At the *equilibrium lattice constant* a_{eq} of each element, the order of elastic softness $q(\hat{G})$ is guaranteed by harmonic elasticity (i.e., the 100 and 111 directions must be the elastic extrema): For Cu and Al, (100) is the softest and (111) the hardest, while for Zn, (111) is the softest and (100) the hardest direction. (iii) The order of elastic softness can change for substrate lattice constants which differ from a_{eq}. For example, a 2% compression of Al is softer along (110) than along (100), while at the equilibrium the opposite is true.

The instability of fcc-Zn is manifested by the softening of $q(111)$ and by negative q values along the (110) and (111) directions for lattice parameters up to about 5% smaller than the equilibrium fcc Zn lattice constant. This observation is understandable in light of Fig. 1(b): It shows that (111) distortions of fcc Zn lower the total energy as c/a increases from 1. Such $c/a>1$ values in Fig. 1 correspond in Fig. 2 to lattice constants below the equilibrium a_{eq} value. Thus, $\Delta E^{\text{epi}}[a,(111)]$ is negative in this lattice parameter range. Since, however, $\Delta E^{\text{bulk}}(a)$ is always positive, $q(111)<0$ for $a<a_{\text{eq}}$.

B. The alloy constituent strain energies

The calculated elemental epitaxial energies can now be used to determine the *constituent strain energy* that is defined as the equilibrium value of the composition-weighted sum of the epitaxial energies of A and B:

$$\Delta E_{CS}^{\text{eq}}(x,\hat{G})=\min_{a_p}[x\Delta E_A^{\text{epi}}(a_p,\hat{G})+(1-x)\Delta E_B^{\text{epi}}(a_p,\hat{G})], \tag{2}$$

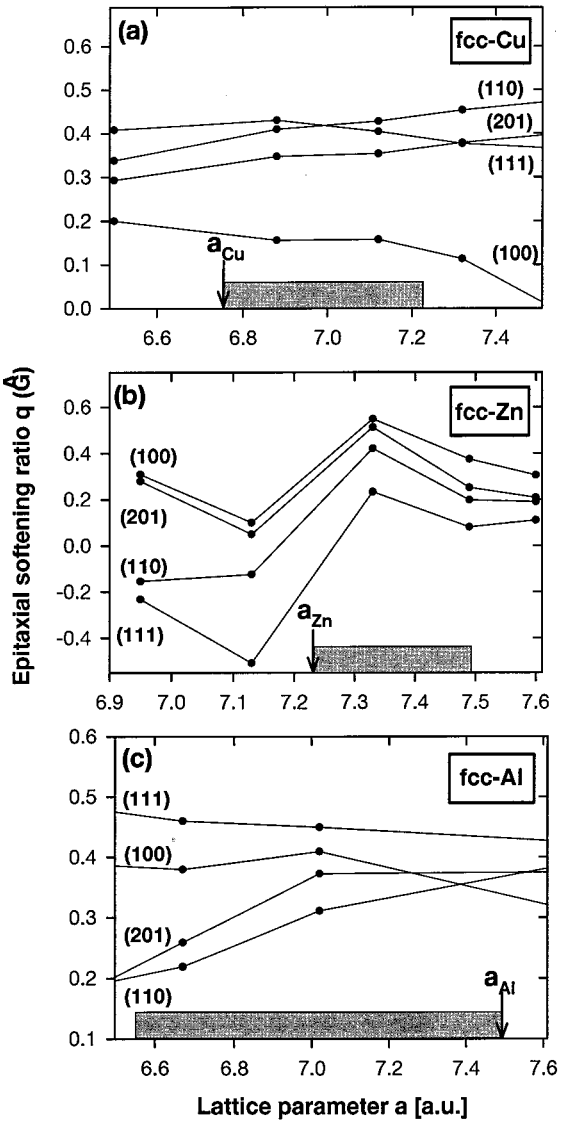

FIG. 2. Epitaxial softening function $q(a,\hat{G})$, Eq. (1), for fcc-Cu, fcc-Zn, and fcc-Al calculated via LDA. The shaded areas mark the lattice parameter range between the individual components of the considered alloy. The q-factor values for the (110) and (111) direction of Zn become negative for lattice parameter values smaller than the fcc-Zn equilibrium value. Arrows denote the position of the equilibrium lattice constant a_{eq} of each element. The lines are drawn merely to guide the eye.

where $a_p(x)$ is the lattice constant that minimizes $\Delta E_{CS}^{\mathrm{eq}}$ at each x. Figure 3 presents the constituent strain energy for $\mathrm{Al}_x\mathrm{Cu}_{1-x}$ and $\mathrm{Al}_x\mathrm{Zn}_{1-x}$ as function of the Al composition for different directions.[41] We see that (i) all strain energies are about an order of magnitude smaller for Al-Zn than for Al-Cu. In fact, the strain energy in $\mathrm{Al}_x\mathrm{Zn}_{1-x}$ does not exceed a value of 5 meV/atom for any direction. (ii) The strain energies of the $\mathrm{Al}_x\mathrm{Zn}_{1-x}$ alloy are characterized by the existence of an elastically soft (111) direction and an elastically hard (100) direction. In contrast, for $\mathrm{Al}_x\mathrm{Cu}_{1-x}$ the (111) direction is the hardest up to $x=0.70$, while (100) is the elastically softest direction between 25 to 100 % Al. The different directional strain behavior of $\mathrm{Al}_x\mathrm{Zn}_{1-x}$ and $\mathrm{Al}_x\mathrm{Cu}_{1-x}$ alloys can be illustrated by a three-dimensional parametrization of the constituent strain. Figure 4 shows the constituent

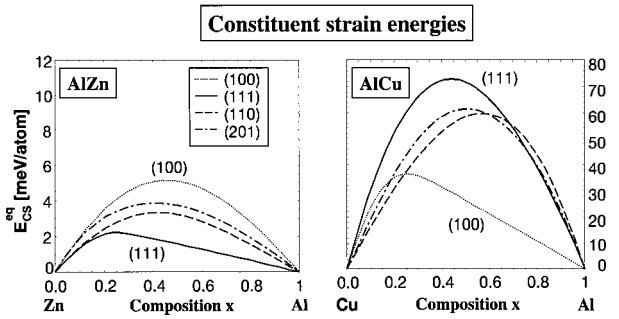

FIG. 3. Constituent strain energies $\Delta E_{CS}^{\mathrm{eq}}$, Eq. (2), for $\mathrm{Al}_x\mathrm{Zn}_{1-x}$ and $\mathrm{Al}_x\mathrm{Cu}_{1-x}$ as function of composition for different directions. The energy values are about an order of magnitude larger for $\mathrm{Al}_x\mathrm{Cu}_{1-x}$ than for $\mathrm{Al}_x\mathrm{Zn}_{1-x}$. All calculated energy differences are given with repsect to the ideal undistorted fcc-crystal of Cu, Al, and Zn.

strain parametrized in terms of a sum of cubic harmonics[42] for a concentration of 90% Al. The distance from the surface to the center of the cube represents the amount of the strain energy for a given orientation. It can be seen that for Al-Cu the figure has a ''depression'' in the very soft (100) direction. In contrast, Al-Zn has the largest extension and therefore, the largest strain energy in the (100) direction, but the smallest extension in the (111) direction.

C. Formation enthalpies of ordered structures

The *formation enthalpy* $\Delta H_f(x,\sigma)$ of an ordered A_pB_q bulk compound is defined as the energy gain or loss with respect to the bulk constituents at their equilibrium lattice constants

$$\Delta H_f(x,\sigma)=E^{\mathrm{tot}}(A_pB_q,\sigma)-xE_A^{\mathrm{tot}}(a_A)-(1-x)E_B^{\mathrm{tot}}(a_B). \tag{3}$$

Here, σ denotes the type or ordered structure, and a_A and a_B

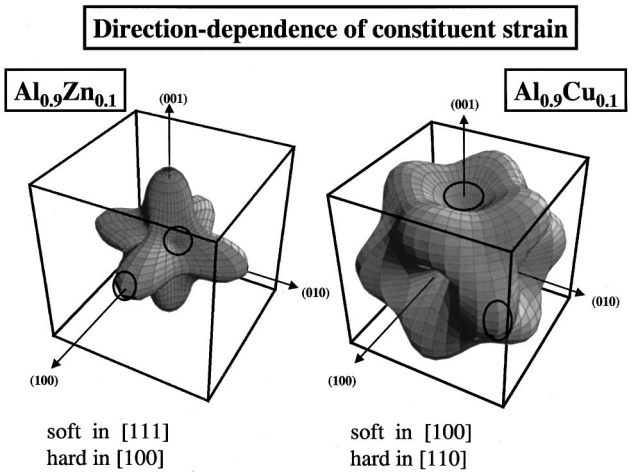

FIG. 4. Parametric three dimensional presentation of the constituent strain $\Delta E_{CS}^{\mathrm{eq}}$, Eq. (2), for a composition of 90% Al. The distance from the surface to the center of the cube represents the amount of the strain energy. The figure demonstrates the different behavior of Al-Zn and Al-Cu. While the (100) direction is the hardest for $\mathrm{Al}_x\mathrm{Zn}_{1-x}$, it is the softest direction for $\mathrm{Al}_x\mathrm{Cu}_{1-x}$.

TABLE I. Cluster expansion fit for Al-Zn. The compounds are sorted by superlattice direction and composition. Compounds marked by a star are not input structures of the cluster expansion fit, but represent prediction. While the ''average fit error'' gives the standard deviation of cluster expansion formation enthalpies of input structures, the ''average prediction error'' represents the standard deviation of all predicted structures. The ''maximum error'' is the largest deviation between the cluster expansion and LDA values of all considered structures.

Average fit error (CE, 26 structures): 1.51 meV
Average prediction error (9 predictions*): 2.16 meV
Maximum error: 4.06 meV

		Direction					
Stoich.	x_{Al}	**(100)**	**(110)**	**(111)**	**(201)**	**(311)**	**others**
Zn	0.0						fcc
direct:							0.0
CE:							+0.6
$AlZn_3$	0.25		$Y3*$	$V3$	$D0_{22}b$	$W3$	$L1_2$
			24.8	4.3	13.3	9.0	5.3
			24.2	3.7	12.5	11.0	10.2
$AlZn_2$	0.333	$\beta 2$	$\gamma 2$	$\alpha 2$			
		14.9	17.7	2.0			
		18.3	21.3	3.3			
Al_2Zn_3	0.40	$Z7*$					
		7.0					
		7.2					
$AlZn$	0.50	$L1_0$		$L1_1$			
		23.5		7.4			
		26.9		9.9			
Al_2Zn_2	0.50	$Z2$	$Y2$	$V2$	$CH(40)$	$W2$	
		9.0	24.6	4.8	24.8	18.6	
		9.6	26.8	7.3	28.8	22.3	
Al_3Zn_3	0.50	$Z6*$	$Y6*$	$V6$			
		6.2	18.8	2.8			
		5.7	16.4	3.2			
Al_4Zn_4	0.50			$V8*$			$SQS8*$
				1.8			18.4
				1.7			20.9
Al_3Zn_2	0.60	$Z5*$					
		6.0					
		6.2					
Al_2Zn	0.667	$\beta 1$	$\gamma 1$	$\alpha 1$			
		17.4	32.6	15.9			
		20.4	33.7	16.7			
Al_3Zn	0.75	$Z1$	$Y1*$	$V1$	$D0_{22}a$	$W1*$	$L1_2$
		10.2	26.0	14.6	27.6	23.0	35.1
		14.1	27.2	12.7	32.6	25.8	34.9
Al_7Zn	0.875						$D7$
							10.7
							12.4
Al	1.00						fcc
							0.0
							-0.6

are the equilibrium lattice constants of the bulk elements A and B. $E_A^{\mathrm{tot}}(a_A)$ and $E_B^{\mathrm{tot}}(a_B)$ are the total energies of A and B, respectively. If $\Delta H_f(x,\sigma)<0$, the compound lies energetically below phase separation, while for a positive value of $\Delta H_f(x,\sigma)$ the phase separated state is favored over the compound.

The formation enthalpies for Al_pZn_q ordered compounds were calculated here using the pseudopotential method. Enthalpies for Al_pCu_q were calculated in Ref. 29 using the LAPW method. Appendix A gives the details of the calculation methods. All formation enthalpies correspond to *geometrically fully relaxed compounds*, i.e., structures were optimized (consistent with the symmetry of the structure) with respect to unit cell vectors, atomic displacements and volume of the unit cell. Indeed, earlier investigations on Cu-Au,[44] Cu-Pd,[44,46] semiconductor alloys,[16,46–48] and Al-Cu (Ref. 29) have clearly demonstrated that inclusion of atomic relaxations in compounds is essential to yield correct physical conclusions. The compounds we considered are defined in Table I in terms of their stoichiometry (e.g., Al_2Zn_3) and superlattice description [e.g., ''Z7'' is a label for a (100) superlattice with 2 monolayers of Al followed by 3 mono-

TABLE II. Cluster expansion fit for Al-Cu (see Table I for details).

Average fit error (CE, 41 structures): 8.24 meV
Average prediction error (0 predictions): —
Maximum error: 41.84 meV

Stoich.	x_{Al}	Direction (100)	(110)	(111)	(201)	(311)	others	others
Cu	0.0						fcc	
direct:							0.0	
CE:							-4.4	
$AlCu_8$	0.111						Ni_8Nb_b	
							-90.8	
							-106.3	
$AlCu_7$	0.125						$D7_b$	
							-93.1	
							-108.7	
$AlCu_3$	0.25	$Z3$	$Y3$	$V3$	$D0_{22}b$		$L1_2$	$SQS14b*$
		-148.2	-143.0	-29.6	-201.7		-193.7	-118.9
		-133.3	-164.6	-51.6	-223.3		-169.3	-129.1
Al_2Cu_6	0.25						$LPS3b*$	$D023$
							-196.8	-199.3
							-191.9	-200.2
Al_3Cu_9	0.25						$LPS21b$	
							-199.7	
							-206.5	
$AlCu_2$	0.333	$\beta 2$	$\gamma 2$	$\alpha 2$				
		-222.5	-215.8	-59.4				
		-180.7	-210.6	-80.6				
$AlCu$	0.50	$L1_0$		$L1_1$				
		-164.0		-112.9				
		-173.4		-112.7				
Al_2Cu_2	0.50	$Z2$	$Y2$	$V2$	$CH(40)$	$W2$		
		-74.0	-140.8	-33.5	-128.8	-124.7		
		-92.6	-110.0	-51.4	-111.2	-117.9		
Al_2Cu	0.667	$\beta 1$	$\gamma 1$	$\alpha 1$				
		-100.1	-71.1	-102.1				
		-111.3	-77.7	-89.9				
$Al_{11}Cu_4$	0.733						$r2 \times r2$	
							-20.5	
							-24.9	
Al_3Cu	0.75	$Z1$	$Y1$	$V1$	$D0_{22}a*$		$L1_2$	$SQS14a*$
		-96.2	-32.5	-51.2	-25.9		-23.1	-52.6
		-93.2	-47.9	-64.7	-36.6		-11.3	-46.7
Al_6Cu_2	0.75	$Z8.2$						
		-49.4						
		-41.0						
Al_7Cu	0.875	$Z8$					$D7$	$r5 \times r5$
		-40.7					+2.4	-64.9
		-42.0					+14.7	-84.0
$Al_{14}Cu_2$	0.875	$Z16.2$						
		-14.0						
		-18.9						
Al_8Cu	0.888						Ni_8Nb_a	
							-15.4	
							-6.5	
$Al_{15}Cu$	0.938	$Z16$					$D16$	
		-19.1					+3.2	
		-20.0					+19.8	
Al	1.00						fcc	
							0.0	
							-1.4	

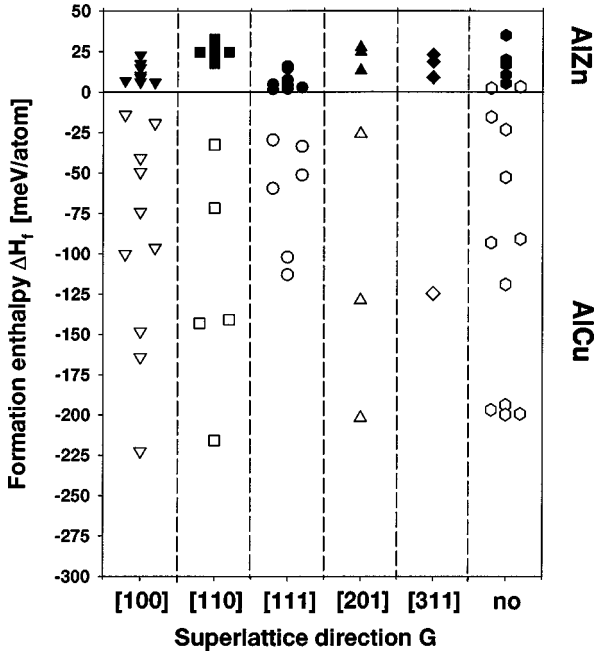

FIG. 5. Fully relaxed LDA formation enthalpies ΔH_f for all considered Al_pZn_q and Al_pCu_q ordered compounds sorted by superlattice direction. While the Al_pZn_q compounds have exclusively positive formation enthalpies, the Al_pCu_q compounds possess nearly all negative formation enthalpies.

layers of Zn]. The calculated ΔH_f are given in Tables I and II and plotted in Fig. 5. We note the following:

(i) While for Al_pCu_q compounds nearly all formation enthalpies are negative, they are exclusively positive for Al_pZn_q. This already characterizes Al-Cu as ordering system, and Al-Zn as phase separating system. The formation enthalpies of Al_pCu_q compounds range between -222.5 meV/atom to $+3.2$ meV/atom, while for Al_pZn_q they range only between $+1.8$ meV/atom to $+35.1$ meV/atom.

(ii) Formation enthalpies for Al_pZn_q compounds with layer ordering along the (111) direction are smallest. This is evident in Fig. 6 which shows all directly calculated formation enthalpies of Al_pZn_q compounds and can be interpreted as a consequence of the unusually low constituent strain energy.

(iii) The formation enthalpies of Al-Zn (110) superlattices are relatively large, even larger than along the (100) superlattices, although Al-Zn also appears to be very soft along (110) (see Fig. 3).

To understand the trends in formation enthalpies we will use the following rough (and admittedly, nonunique) decomposition: We describe the formation enthalpy of any structure as the sum of the constituent strain energy of Eq. (2) and the relaxed ''chemical energy'' including all other contributions,

$$\Delta H_f(x,\sigma) = \Delta E_{CS}^{\mathrm{eq}}(\sigma) + \Delta E_{\mathrm{chem}}(x,\sigma). \tag{4}$$

The partitioning of Eq. (4) leads to the conclusion that for Al_pZn_q compounds ΔE_{chem} on the average must be more positive for structures ordered along (110) than (111). Taking all directly calculated formation enthalpies of ordered compounds along (111) and (110) into account we get average values of $\Delta E_{\mathrm{chem}}(111) = 6.6$ meV/atom and $\Delta E_{\mathrm{chem}}(110) = 24.5$ meV/atom. The averages of the constituent strain energy for considered superlattices amount to $\Delta E_{CS}^{\mathrm{eq}}(\sigma)(111) = 1.1$ meV/atom and $\Delta E_{CS}^{\mathrm{eq}}(\sigma)(110) = 1.6$ meV/atom. In other words, for ''(111) compounds'' even the very soft strain energy gives a fractionally larger contribution to the formation enthalpies shown in Fig. 6, while the fractional contribution of strain to formation enthalpies along (110) is relatively small.

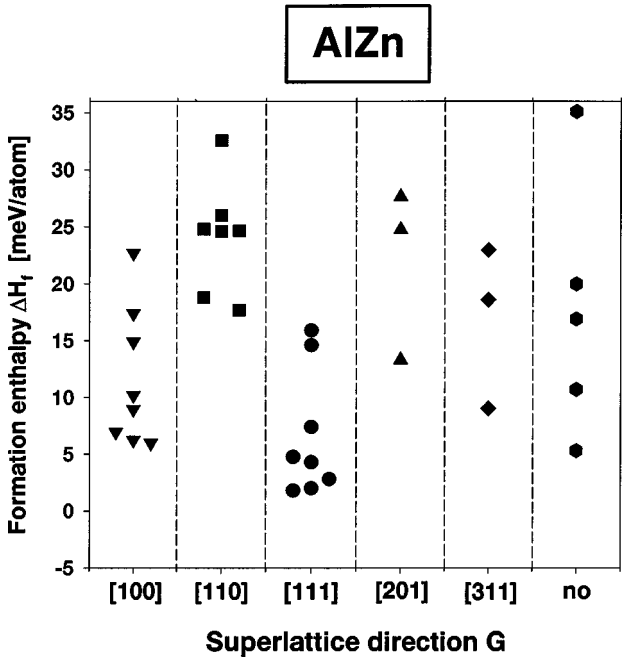

FIG. 6. Fully relaxed LDA formation enthalpies ΔH_f for Al_pZn_q compounds: The smallest values are found for compounds which are superlattices along the (111) direction.

D. A detour: The need to use geometrically equivalent *k* points in evaluating formation enthalpies

The small formation enthalpies in Al_pZn_q demand extremely careful convergence. In addition to convergence with respect to the basis set, one needs to assure convergence with respect to *k* points. Considering Eq. (3), we see that one needs to converge the *k* representation for a compound A_pB_q as well as for the elemental constituents *A* and *B*. The standard way of accomplishing this is to increase the number of *k* points in all 3 systems until convergence is obtained. This can be done using any method of Brillouin zone sampling, e.g., Chadi-Cohen[49] or Monkhorst-Pack.[50] The disadvantage of this approach is that it requires *absolute k* point convergence for *A*, *B* and separately, for A_pB_q. An alternative method is to take advantage of *relative k* point convergence.[51]

The idea is to sample the Brillouin zone *equivalently* for *A*, *B* and for A_pB_q. This could be done by considering A_pA_q, B_pB_q, and A_pB_q as isostructural solids and sample the Brillouin zone of all equally. Then, any relative *k*-point sampling error cancels out. This is called the *method of equivalent k points*.[51] In practice, we do not have to calculate the total energies of A_pA_q and B_pB_q, but we can calculate instead the energies of *A* and *B*, at suitably folded-in *k* points.

TABLE III. Influence of k point set on formation enthalpies ΔH_f and epitaxial energies ΔE^{epi} of Al-Zn: The table compares equivalent (Ref. 51) and regular mesh (Ref. 50) k-point sets. $N\times N\times N$ represents the number of k points in the Brillouin-zone before reduction by symmetry. Structures are defined in Table I.

System	Equivalent k points ΔH_f (meV/atom)			Regular mesh ΔH_f (meV/atom)		
	$N=8$	$N=10$	$N=12$	$N=8$	$N=10$	$N=12$
epi: Zn(100)	+14.6	+15.5	+15.6	+4.8	+20.8	+11.7
epi: Al(110)	+4.3	+4.5	+4.5	−2.1	+10.2	+8.7
epi: Zn(111)	−5.3	+3.3	+3.2	−2.6	+0.9	+3.0
ΔH_f: $L1_2$ (Al_3Zn)	+33.8	+33.1	+34.2	+34.1	+33.8	+33.7
ΔH_f: $L1_0$ (AlZn)	+22.7	+23.6	+23.5	+15.7	+18.1	+20.0
ΔH_f: $L1_1$ (AlZn)	+6.5	+9.1	+9.4	−4.6	+3.2	+4.0

For comparison three epitaxial energies as well as three formation enthalpies were calculated using $N\times N\times N$ regular (Monkhorst-Pack) and equivalent k points for $N=8,10,12$. Here, $N\times N\times N$ is the number of k points in the first Brillouin-zone before reduction by symmetry. The chosen epitaxial systems are Zn(100) and Zn (111) relaxed at $a=7.50$ a.u. ($a_{\text{eq}}=7.23$ a.u.) as well as Al(110) relaxed at $a=7.33$ a.u. ($a_{\text{eq}}=7.50$ a.u.). The three ordered compounds are $L1_2$, which does not allow any cell-vector distortions, as well as $L1_0$ and $L1_1$ allowing distortions along the c-axes in the (100) and (111) directions, respectively. The results are shown in Table III: It can be seen that the ΔH_f values for equivalent sets converge much faster than using regular sets. Indeed, even a $10\times10\times10$ regular mesh k-point set for most cases (except $L1_2$) is not sufficient. For equivalent k-points a set of $10\times10\times10$ k points represents the smallest acceptable choice especially for distortions along (111).

To determine the minimum number of equivalent k points needed we calculate ΔH_f for superlattices along (111) direction. The reason for selecting this ordering direction is that atomic movements along (111) are very large due to the unusual epitaxial softness along this direction. These tests (Table IV) show that sometimes even $12\times12\times12$ equivalent k points are not sufficient for convergence: While for the $L1_2$, $L1_1$, and $V2$ structures, the use of $8\times8\times8$ k points already leads to stable results, for the $\alpha2$, $V3$, $V6$, and $V8$ structures this is definitely not the case. For example, ΔH_f for $\alpha2$ and $V6$ are −4.1 and −9.9 meV/atom using $12\times12\times12$ while using $18\times18\times18$ gives +2.0 and +2.8 meV/atom, respectively. As a result, a $12\times12\times12$ set of k points would erroneously predict the Al-Zn system to be ordering-type along (111), but phase separating along all other directions. This k-point problem is connected to unusual small formation enthalpies of Al_xZn_{1-x}. It should be mentioned that the problem described only appears for compounds with equivalent superlattices along (111), i.e., for compounds showing large cell-vector distortions and atomic movements. Formation enthalpies calculated for other compounds do not show such a high sensitivity to the number of k points.

TABLE IV. Formation enthalpies [meV/atom] of Al-Zn for different numbers of equivalent k points. $N\times N\times N$ represents the number of k points in the Brillouin-zone before reduction by symmetry. Structures are defined in Table I.

Structure	Stoichiometry	$N\times N\times N$ k points				
		$N=8$	$N=10$	$N=12$	$N=16$	$N=18$
$L1_2$	Al_3Zn	+33.8	+33.1	+34.2	+34.9	+35.1
$L1_1$	AlZn	+6.5	+9.1	+9.4	+8.0	+7.4
V_2	Al_2Zn_2	+2.9		+4.3	+4.8	
α_2	$AlZn_2$			−4.1		+2.0
V_3	$AlZn_3$	−5.3		−3.5	+4.3	
V_6	Al_3Zn_3			−9.9		+2.8
V_8	Al_4Zn_4	−10.6			+1.8	

IV. THERMODYNAMIC QUANTITIES

To calculate finite temperature, thermodynamic properties with first principles accuracy, pair- and multibody effective cluster interactions are needed as input for Monte Carlo simulations. These interactions are generated by use of a mixed-space cluster expansion with directly calculated LDA strain energies and formation enthalpies as input. We next describe the construction of the cluster expansion for Al-Cu and Al-Zn.

A. The mixed space cluster expansion for Al-Zn and Al-Cu

It has been demonstrated[42–44,29] that a *mixed-space cluster expansion*[16,17] is an efficient and accurate tool for calculating ground states, mixing enthalpies, superlattice energies, phase diagrams, and short-range order. This expansion allows a fast and precise prediction of formation enthalpies for any arbitrary atomically relaxed configuration σ expressed in the form

$$\Delta H_{CE}(\sigma)=\sum_{\mathbf{k}} J_{\text{pair}}(\mathbf{k})\left|S(\mathbf{k},\sigma)\right|^2 + \sum_{f}^{MB} D_f J_f \overline{\Pi}_f(\sigma)+\Delta E_{CS}(\sigma). \qquad (5)$$

The first term includes all pair figures where $J_{\text{pair}}(\mathbf{k})$ and $S(\mathbf{k},\sigma)$ are the lattice Fourier transforms of real space interactions and spin-occupation variables. The second term represents many-body interactions and runs over symmetry inequivalent clusters consisting of three or more lattice sites. D_f stands for the number of equivalent cluster per lattice site,

and $\overline{\Pi}_f(\sigma)$ are structure-dependent geometrical coefficients. The last term represents the constituent strain energy of the structure σ, $\Delta E_{CS}(\sigma)$, and can be calculated by expanding the equilibrium constituent strain energy $\Delta E^{\rm eq}_{CS}(x,\hat{k})$ in Eq. (2), as[16,45]

$$\Delta E_{CS}(\sigma)=\sum_{\mathbf{k}} J_{CS}(x,\hat{k})|S(\mathbf{k},\sigma)|^2 \tag{6}$$

with

$$J_{CS}(x,\hat{k})=\frac{\Delta E^{\rm eq}_{CS}(x,\hat{k})}{4x(1-x)}. \tag{7}$$

For more details, see Refs. 16,17,42–44.

This method has been applied previously to the Al-Cu system.[29] Here, we apply it to Al-Zn and contrast the results of energetic and thermodynamic properties with those of Al-Cu. To determine the coefficients $\{J_{\rm pair}(\mathbf{k})\}$, and $\{J_f\}$ of the cluster expansion we need as input the formation enthalpies $\Delta H_f(A_pB_q)$ of ordered compounds which were discussed in detail in Sec. III C. The real-space pair and multi-body interactions are fit to the N_σ formation enthalpies $\{\Delta H_f\}$, minimizing the root mean square (rms) error $\Delta_{\rm rms}$:

$$\Delta^2_{\rm rms}=\frac{1}{N_\sigma}\sum_{\sigma} w_\sigma[\Delta H_{CE}(\sigma)-\Delta H_{\rm LDA}(\sigma)]^2$$

$$+\frac{t}{\alpha}\sum_{\mathbf{k}} J_{\rm pair}(\mathbf{k})[-\nabla^2_{\mathbf{k}}]^{\lambda/2}J_{\rm pair}(\mathbf{k}), \tag{8}$$

where λ and t are free parameters and α is a normalization constant.[16] This **k**-space smoothness criterion automatically selects optimally short-ranged pair interactions. Then, a large number of different sets of three and four-body figures is tested as to whether it improves the rms error of the overall fit. An individual multi-body interaction is only added to the fit if it strongly decreases $\Delta_{\rm rms}$. In this sense, it is important to check the stability of the cluster expansion as measured by a change in other multibody interactions upon the addition of a particular figure. Table I shows the input formation enthalpies ΔH_f and the fitted enthalpies for Al-Zn. All enthalpies that have an asterisk denote structures not used in the fit. The average error of fitting $N_\sigma=26$ enthalpies is 1.5 meV whereas the error for the 9 other structures not used in the fit is 2.5 meV. Figure 7 gives the pair and selected multibody interactions used for the Al-Zn system. It can be seen that pair interactions converge rapidly, so that a consideration of 15–20 pair interactions is sufficient. (For more details on construction of a mixed-space cluster-expansion, see Ref. 43.)

The mixed-space cluster-expansion for Al-Cu is given in Table II. Because this expansion was constructed to study precipitates in Al-rich alloys,[29] the Al-rich compounds were heavily weighted in the fitting procedure, at the expense of larger errors for Cu-rich compounds. The average fit error is a factor of two larger than for Al-Zn, partly a reflection of the larger formation enthalpies in Al-Cu. While it is possible to dramatically reduce the fit error in Al-Cu by giving Cu-rich compounds more weight in the cluster-expansion fit, this leads to an incorrect ground state and therefore, to incorrect

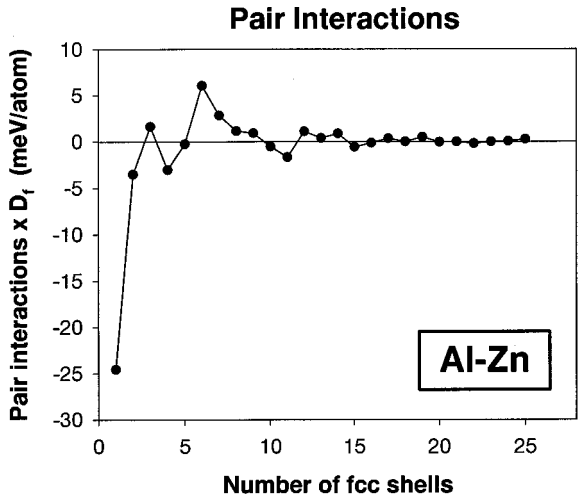

FIG. 7. Pair and multibody effective cluster interactions for Al-Zn deduced from the fit of Table I. The symbols characterize individual multibody interactions: ''3'' stands for three- and ''4'' for four-body interactions. In general, the distance between atoms increases with the letter, i.e., for example, ''J'' means only nearest neighbors, ''K'' nearest neighbors and one second nearest neighbor, etc.

physical properties regarding short-range order behavior of the alloy system. This example makes clear that the average fit error of a cluster-expansion cannot be used as an absolute measure for its quality. Moreover, the stability of the fit and the correct ground state behavior are more important, for the *predictive* abilities of the expansion.[52]

B. Mixing enthalpies of disordered and random alloy

The effective cluster interactions of Al-Zn were used to calculate the mixing enthalpy for a disordered alloy by Monte Carlo simulations in the canonical ensemble. Test calculations for different numbers of atoms found that the use of a fcc grid consisting of $20\times20\times20$ atoms is more than sufficient. The temperature $T=643K$ was chosen, because an earlier study by Mey[53] done for the same temperature opens the possibility for a direct comparison. This earlier investigation used a polynomial description which was adjusted for a best fit to all experimental information using a least squares program [CALPHAD I (Ref. 54)]. The calculation was made

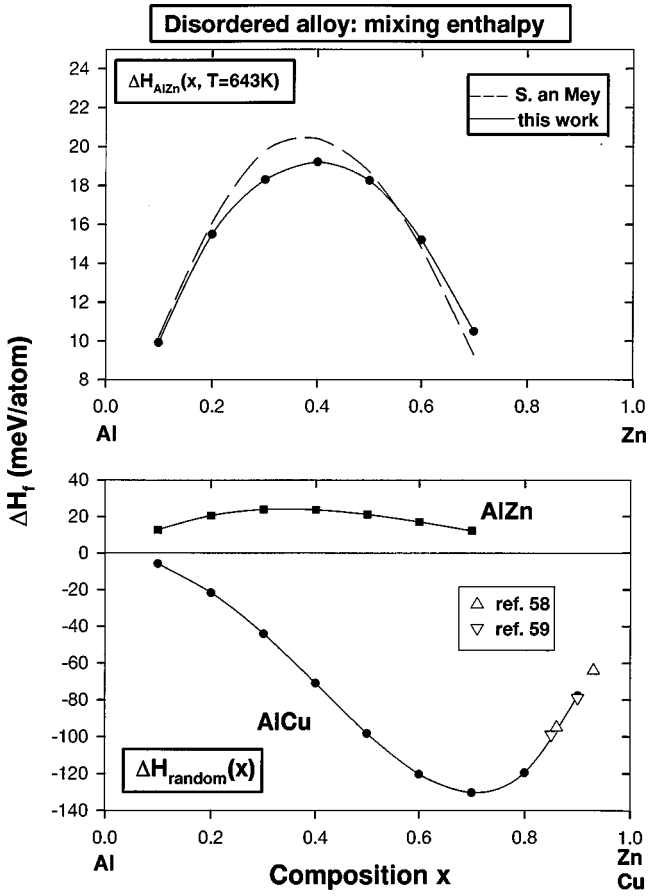

FIG. 8. (a) Calculated mixing enthalpy ΔH of Al_xZn_{1-x} at $T=643$ K as function of composition. The dashed line defines the result of a study using CALPHAD from Ref. 53, while the solid line is our calculated first-principles mixing enthalpy $\Delta H_{\mathrm{AlZn}}(x,643\ \mathrm{K})$. (b) Calculated mixing enthalpy of the random alloy as function of composition for Al_xZn_{1-x} and Al_xCu_{1-x}, and comparison with measured values of Cu-rich alloys taken from Refs. 58,59.

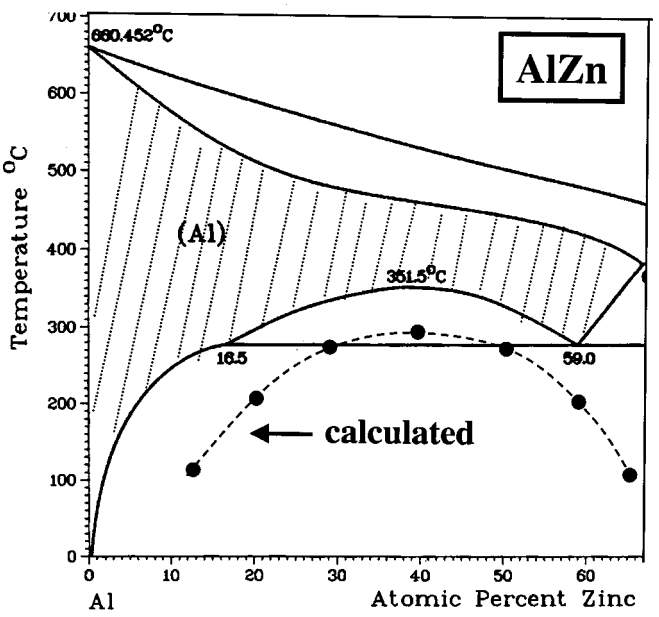

FIG. 9. Calculated coherent fcc-miscibility gap of Al_xZn_{1-x}. The experimental phase diagram, which shows the *incoherent* miscibility gap, is taken from Ref. 15.

for the fcc solid solution relative to fcc constituents, i.e., the fcc-hcp energy difference for Zn was already subtracted. Our calculated first-principles mixing enthalpy $\Delta H_{\mathrm{AlZn}}(x,643\ \mathrm{K})$ and the phenomenological fit to experiment of an Mey[53] are compared in Fig. 8(a). The two curves agree very well: Both show a maximum around 40% Zn with a corresponding mixing enthalpy of about 20 meV/atom. A comparison to individual experimental studies of the fcc phase appears to be very difficult, because their results differ profoundly: For example, while calometric studies of Wittig and Schöffl[55] ($T=643$ K) and Connel and Downie[56] ($T=637$ K) lead to a maximum in the enthalpy of mixing at about 25% Zn, electromagnetic field studies by Hilliard, Averbach, and Cohen[57] ($T=653$ K) find a maximum around 60% Zn. To our knowledge these discrepancies for the thermodynamic properties of the fcc solid solution are not yet clarified; hence, future experimental studies would be desirable.

We also have calculated the mixing enthalpy of the configurationally-random alloy: Monte Carlo simulations were performed for extremely high temperatures (e.g., $T=50\,000$ K) where almost all atomic exchanges of the Metropolis algorithm are accepted. This simulation samples the configuration space in an unbiased manner, and gives the energy of the configurationally-random state. The composition dependence of $\Delta H(\mathrm{random})$ is given in the lower part of Fig. 8. The difference between the results of Fig. 8(a) and those in Fig. 8(b) are due to the energetic effect of short-range order in the solid solution. For the phase separating alloy system Al_xZn_{1-x} all values are positive exhibiting a maximum around 40% Zn, while for the ordering system Al_xCu_{1-x} all values are negative exhibiting a minimum around 30% Cu. The mixing enthalpy of the Al_xZn_{1-x} random alloy at the maximum amounts to $+24$ meV/atom, while the mixing enthalpy of the Al_xCu_{1-x} random alloy at the minimum amounts to -130 meV/atom. These calculated enthalpies (without the effects of short-range order) may be compared with measured values[58,59] for disordered Cu-rich alloys which are also shown in Fig. 8. As can be seen, the agreement is very good, especially, if we consider that the theoretical values are for the fully random alloy and a discussion of the cited experimental investigations by Hultgren[13] gives an error estimate of ± 30 meV/atom for these measured values.

The limited solubility of Cu in Al means that it is not possible to compare the entire curve in Fig. 8 with experiment, but rather only the Al-rich dilute limit. The dilute heat of solution for Cu in Al can be computed from our cluster expansion approach: The calculated value for an $Al_{0.99}Cu_{0.01}$ alloy is $\Delta H_{\mathrm{solution}}=-50$ meV/Cu atom for the random alloy, and $\Delta H_{\mathrm{solution}}(T=700\ \mathrm{K})=-70$ meV/Cu atom when short-range order is taken into account. Both of these values are extremely small (in magnitude) compared to the formation enthalpies of ordered Al-rich compounds, e.g., $\Delta H(Z1)=-96.2$ meV/atom $=-385$ meV/Cu atom, nearly an order of magnitude larger than the heat of solution. The smallness of the heat of solution is due to the asymmetric shape of the random alloy energy in Fig. 8. The curvature of the random alloy energy changes sign and the mixing energy nearly becomes positive for Al-rich alloys. Interestingly, this asymmetry also exists in the measured enthalpy of liquid

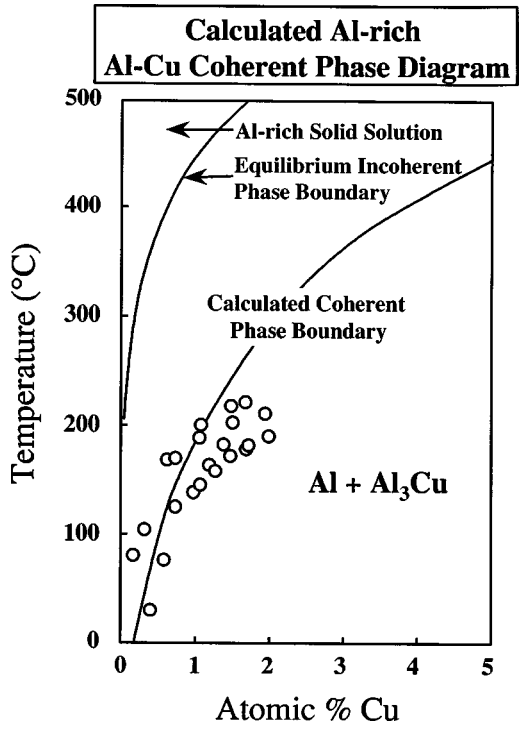

FIG. 10. Calculated coherent phase boundary between Al-rich solid solution and predicted Al_3Cu coherent ground state and comparison to measured values of coherent precipitation solvus curves taken from Ref. 75.

Al-Cu.[7] The smallness of our calculated heats of solution is consistent with the measured heat of solution[60] $\Delta H_{\text{solution}} = -35$ meV/Cu atom.

Naturally, our random alloy calculation represents a solid-state fcc solid solution, but it is nevertheless interesting to compare with the measured formation enthalpies of liquid alloys: Assessed data and unpublished results (see Ref. 7) give a mixing enthalpy for liquid Al-Cu (with respect to liquid constituents) which is asymmetric towards Cu-rich compositions with a minimum value of ~ -100 meV/atom, consistent with our solid-state calculations. Experimental[13,61] and theoretical[53] investigations of the Al-Zn liquid alloy find a maximum mixing enthalpy between 25 and 27 meV/atom at 50% Zn in very good agreement to our calculations of the solid solution.

C. Coherent phase boundaries

As stated in the Introduction, a special property of Al-Zn is the large solubility of Zn in Al and the existence of a miscibility gap in the solid solution (Fig. 9). We calculated the coherent fcc miscibility gap by annealing the solid solution, lowering the temperature, and looking for the temperature at which the specific heat shows a maximum. These calculations were done for a number of different Zn concentrations. The resulting curve is given in Fig. 9, the experimental phase diagram is taken from Ref. 15. The coherent miscibility gap is supressed below the incoherent miscibility gap due to the additional elastic energy required to maintain coherence with the fcc matrix.[4,5] We find a coherent critical temperature of $T = 295\,^{\circ}\text{C}$ for about 40% Zn in reasonable agreement to the experimental values of about 318–328 °C (Refs. 18–20) as already discussed in the Introduction.

The equilibrium Al-Cu phase diagram shows no miscibility gap. Rather, the Al-rich portion has a small region of solubility of Cu in Al followed by an incoherent two-phase field of this solid solution with the equilibrium (non-fcc-based) Al_2Cu (θ) compound. The details of the Al-rich portion of the coherent phase diagram are related to the structure and ordering of coherent Cu precipitates in Al, which is the source of much experimental controversy.[28] However, recently it has been theoretically predicted (using the methods described in this paper)[29] that the coherent Al-Cu phase diagram possesses an Al-rich Al_3Cu compound. The coherent phase boundary between the Al-rich solid solution and this Al_3Cu compound is shown in Fig. 10. Measurements of the coherent solvus curves are redrawn from Fig. 9 of Ref. 75. Both ''GP'' (Guinier-Preston, or GP1) and θ'' (or GP2) data are redrawn from Ref. 75, however, since it was recently found[29] that these phases are not distinct thermodynamic phases, we have not distinguished the two sets of measured data. In both the Al-Zn and Al-Cu alloys, the agreement between the calculated and measured coherent phase boundaries is quite good, particularly since our calculations involve a statically relaxed, but nonvibrating lattice.

D. Short-range order

The short-range order (SRO) behavior of a system can be described in terms of the Warren-Cowley SRO parameters which are given for shell (lmn) by

$$\alpha_{lmn}(x) = 1 - \frac{P_{lmn}^{A(B)}}{x}, \tag{9}$$

where $P_{lmn}^{A(B)}$ is the conditional probability that given an A atom at the origin, there is a B atom at (lmn). The sign of α indicates qualitatively whether atoms in a given shell prefer to order ($\alpha < 0$) or cluster ($\alpha > 0$). The SRO parameter may be written in terms of the cluster expansion pair correlations as

$$\alpha_{lmn}(x) = \frac{\langle \overline{\Pi}_{lmn} \rangle - q^2}{1 - q^2}, \tag{10}$$

where $q = 2x - 1$ and $\langle \overline{\Pi}_{lmn} \rangle$ is the pair correlation function for shell (lmn). In diffraction experiments the portion of diffuse scattering due to SRO is proportional to the lattice Fourier transform of $\alpha_{lmn}(x)$

$$\alpha(x, \mathbf{k}) = \sum_{lmn}^{n_R} \alpha_{lmn}(x) e^{i \cdot \mathbf{k} \cdot \mathbf{R}_{lmn}}, \tag{11}$$

where n_R stands for the number of real space shells used in the transform. (For more details, see, for example, Refs. 62,63, and references therein; for examples of applications of the mixed-space cluster expansion to SRO in transition-metal and noble-metal alloys, see Ref. 44.)

The SRO of Al_xZn_{1-x} solid solutions was calculated for two different Zn concentrations, namely 10 and 50% Zn at $T = 700$ K (Fig. 11). For these alloys, α_{lmn} were computed by taking thermal averages of the spin products $\langle \overline{\Pi}_{lmn} \rangle$ and then using Eq. (10) to obtain the SRO parameters α_{lmn}. Using a finite number n_R of these real-space shells in Eq. (11), we obtain the SRO in reciprocal space $\alpha(x, \mathbf{k})$ (for

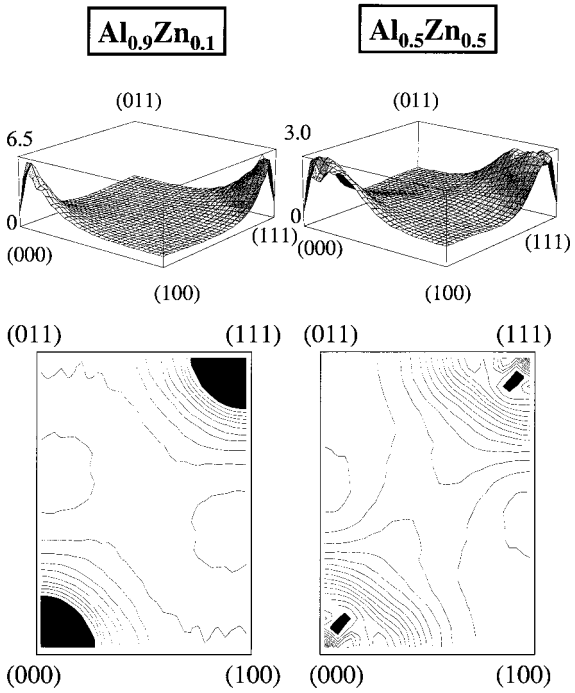

FIG. 11. Short-range order maps of $Al_{0.9}Zn_{0.1}$ (left) and $Al_{0.5}Zn_{0.5}$ (right). Peaks are at Γ and streaks in the SRO intensity along (111) are visible. Clustering tendencies are clearly stronger for 10% than for 50% Zn resulting in a higher intensity value around the Γ point for $Al_{0.9}Zn_{0.1}$. A temperature of $T=700$ K was chosen for the calculations in order to guarantee presence in the solid solution.

more details, see Ref. 44). The SRO in $Al_{0.5}Zn_{0.5}$ shows diffuse intensity at $\Gamma=(000)$, with streaks along the (111) direction. The SRO at Γ is indicative of a clustering tendency in the solid solution, consistent with the miscibility gap in the Al-Zn phase diagram (Fig. 9) and the positive formation enthalpies (Table I). The streaking of the SRO along (111) is a ''fingerprint'' (Table I) of the energetic preference for superlattices along (111), which as we described above, are due to the instability of fcc Zn when distorted rhombohedrally. Therefore, the shape of the SRO peaks in the solid solution can be interpreted as a consequence of the instability of fcc-Zn. The SRO behavior of Al-Zn alloys in the solid solution is also interesting since it can manifest itself at lower temperatures in precipitation experiments. Aging of Al-Zn alloys show (111) faceting of Zn precipitates as well as a crossover at a critical particle size from spherical to oblate ellipsoid, with the short axis in (111) direction.[23,25,26] Upon going to Al-rich compositions, the SRO of $Al_{0.9}Zn_{0.1}$ also peaks at Γ, but the streaking along the (111) direction is diminished. This reduction of the (111) streaks for Al-rich compositions is a consequence of the fact that formation enthalpies of superlattices along (111) become larger (i.e., less stable) with increasing Al concentration. Another interesting point is that the clustering tendency appears to be stronger for $x_{Zn}=0.1$ than $x_{Zn}=0.5$. For the latter the maximum intensity around the Γ point results to be about a factor of 2 lower than for $x_{Zn}=0.1$. A comparison of our theoretical values of the SRO parameter α with those coming from experimental measurements shows a qualitative agreement: Desplat *et al.*[2] performed neutron diffuse scattering measurements on 7 and 17 % Zn single crystals and extracted SRO parameters for the first six nearest neighbor shells. Their results show that α decreases rapidly with distance, and all values are positive as expected for a clustering-type system. Our theoretical values show the same tendency, but are about a factor of 1.5–2.0 larger than the values given by Desplat *et al.* The reason for this discrepancy is not yet clear, so that more theoretical and experimental studies would be desirable. In this connection, our predicted values for the short-range order parameters α for $x_{Zn}=0.1$ and $x_{Zn}=0.5$ at $T=700$ K are given for the first ten shells in Table V.

TABLE V. Calculated SRO parameters for an $Al_{0.9}Zn_{0.1}$ and an $Al_{0.5}Zn_{0.5}$ at $T=700$ K for the first 10 shells.

Shell (lmn)	$Al_{0.9}Zn_{0.1}$	$Al_{0.5}Zn_{0.5}$
0 0 0	1.000	1.000
1 1 0	0.107	0.094
2 0 0	0.079	0.044
2 1 1	0.035	0.018
2 2 0	0.036	0.018
3 1 0	0.021	0.007
2 2 2	0.007	−0.019
3 2 1	0.010	−0.003
4 0 0	0.009	−0.001
3 3 0	0.008	−0.001

The calculated SRO of $Al_{0.98}Cu_{0.02}$ is shown in Fig. 12. Again, the SRO peaks are at the Γ point, indicative of a clustering tendency in the solid solution. However, in Al-Cu the SRO pattern shows streaks along (100) rather than the (111) streaks seen in Al-Zn. The (100) SRO streaks are again a high-temperature reflection of the elastically soft direction of Cu, which manifests itself in low-energy (100)-type superlattices for Al-rich compounds (Table II).

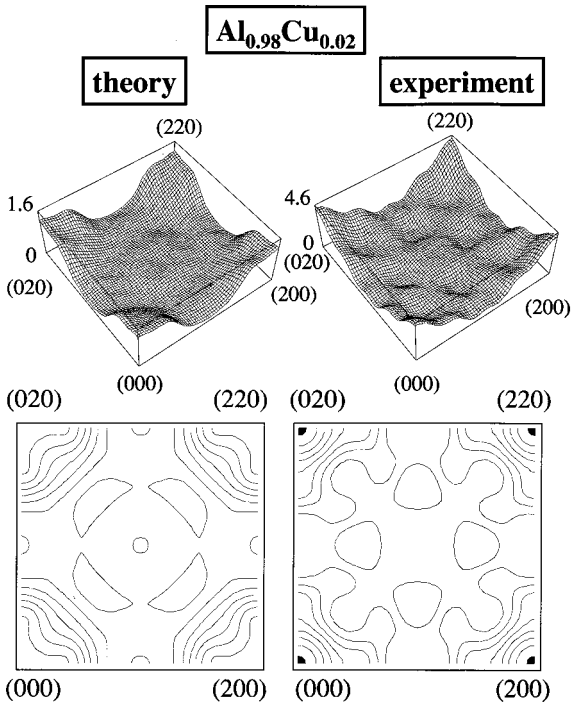

FIG. 12. The calculated and experimental SRO patterns in $Al_{0.98}Cu_{0.02}$. The experimental data are taken from Ref. 8.

TABLE VI. Experimental (Ref. 8) and calculated SRO parameters for an $Al_{0.98}Cu_{0.02}$ alloy, and comparison with SRO parameters of the fully ordered Al_3Cu (Z1) state.

Shell (lmn)	Calculated Al_3Cu_1 ($Z1$)	Calculated $Al_{0.98}Cu_{0.02}$ 650 K	Calculated $Al_{0.98}Cu_{0.02}$ 800 K	Measured $Al_{0.983}Cu_{0.017}$ 793 K
0 0 0	1.000	1.000	1.000	1.019
1 1 0	0.111	0.041	0.029	0.141
2 0 0	0.556	0.029	0.020	0.095
2 1 1	−0.333	−0.002	−0.002	0.012
2 2 0	0.111	−0.005	−0.005	0.014
3 1 0	0.111	−0.001	−0.001	0.032
2 2 2	−0.333	−0.005	−0.004	0.004
3 2 1	−0.333	−0.000	0.0000	0.002
4 0 0	1.000	0.004	0.002	−0.007
3 3 0	0.111	−0.001	−0.001	0.018

One might be surprised by the clustering tendency of the solid solution since almost all the calculated formation enthalpies for ordered compounds (Table II) and mixing energies of random alloys (Fig. 8) are negative. This apparent dichotomy can be explained by examining the predicted coherent ground state of Al_3Cu:[29] this phase is an Al_3Cu_1 (001) superlattice, refered to as ''Z1'' (see Table II). In Table VI SRO parameters are shown for fully ordered Z1, the calculated values for an Al-2%Cu alloy at 650 and 800 K as well as the experimental values at 793 K from Ref. 8, all for the first ten real-space shells. The interesting thing to note is that $\alpha>0$ (indicating clustering) for the first two shells of Z1. In other words, if one only looks ''locally'' at the Z1 structure (within the first two neighbor shells), it looks more like clustering than ordering. Only when the third neighbor shell is taken into account does a negative α appear. For the calculated SRO for Al-Cu, the signs of the first three calculated parameters are in accord with those of Z1, but it can be seen that the calculated SRO parameters decay very rapidly, so that they are practically zero by the time the third neighbor shell is reached. The first and second shells dominate the SRO pattern and produce a Γ-like clustering behavior. Thus, Al-Cu shows a clustering tendency even though the underlying coherent ground states (''Z1'') are ordered compounds. The coherent ground state is an ordered phase which appears locally as ''clustering'' on a short length scale.

Also shown in Table VI is the SRO as measured by diffuse x-ray scattering.[8] The measured SRO pattern also shows a clustering tendency with peaks at the Γ-point and streaks along the elastically soft (100) direction; additionally, it is noteworthy that the measured SRO parameters in Al-Cu (Ref. 8) are much larger (indicating ''more clustering'') than the calculated ones. In fact, the measured SRO parameter for the first shell is even larger than the value for the predicted Al_3Cu fully ordered coherent compound. This large value for the measured SRO parameter is difficult to explain, and interestingly, the same qualitative distinction was found previously between calculated[29] and measured[21] coherent precipitate shapes: The calculated precipitate shapes[29] involve Cu monolayers and ordering of monolayers, and hence are ''less clustered'' than the model deduced from diffuse scattering measurements[21] of thicker multilayer zones. Some authors[72] have demonstrated that diffuse scattering measurements using a limited sampling of reciprocal space (such as that of Ref. 8) can lead to artificially large SRO parameters for precipitation experiments. Additionally, these comparisons of SRO parameters for aged alloys are always clouded by issues of kinetics, aging times, vacancy concentrations, etc. However, for temperatures where the solid solution is in thermodynamic equilibrium, these kinetic issues and ambiguities should not arise in measurements of SRO in the disordered phase. Hence, future work on the SRO of Al-Cu solid solutions would not only be of considerable interest in resolving the discrepancy present in Table VI, but also would shed light on some of the controversy surrounding the models of coherent precipitation in Al-Cu alloys.

V. SUMMARY

Total energy calculations of elemental fcc Zn yield an instability when rhombohedrally distorted along the (111) direction [or orthorhombically distorted along (110)]. This instability leads to unusually small epitaxial energies especially in the (111) direction. Consequently, (111) is the softest elastic direction in fcc-Zn, but the hardest in Cu and Al for small distortions. This unusual property of fcc-Zn is pervasive and strongly influences the physical properties of Al_xZn_{1-x} alloys. Not only for elemental fcc Zn, but also for Al_xZn_{1-x} alloys, (111) is always the softest direction. Therefore, strain energies and formation enthalpies along (111) possess unusually small values compared to all other considered compounds. The small formation enthalpies of superlattices along (111) also affect thermodynamic properties such as the SRO, which shows clustering with streaks of intensity along the (111) direction and sharp peaks at the Γ point. In contrast, for Al-Cu the formation enthalpies are an order of magnitude larger in absolute value, and streaking of SRO intensities along (100) is visible due to the soft (100) direction in Al-Cu for Al-rich compositions.

Effective cluster interactions obtained from a mixed-space cluster expansion were used as input for Monte Carlo simulations to study thermodynamic quantities of both alloy systems. Mixing enthalpies of disordered and random alloys agree very well with most earlier theoretical and experimental data. The calculated coherent phase boundaries of Al_xZn_{1-x} and Al_xCu_{1-x} are also in good agreement with experimental data. The determination of the Al_xZn_{1-x} fcc coherent miscibility gap represents an important prerequisite for a detailed study of precipitate shapes in Al-Zn. Precipitates in Al-Zn are observed as ellipsoidal with a polar axis parallel to the (111) direction.[23,25,26] Even the form of these precipitates could perhaps be controlled by the extremely small (111) strain in Al-Zn and therefore, would be an indirect consequence of the instability of fcc Zn found here. The instability will presumably influence all binary and multicomponent fcc-alloy systems with Zn as one constituent. So, the instability of fcc Zn is generally important towards understanding the constituent strain and precipitation in fcc alloys containing Zn.

ACKNOWLEDGMENTS

The work at NREL was supported by the Office of Science, Basic Energy Sciences, Material Science Division,

U.S. Department of Energy, under Contract No. DE-AC36-98-GO10337.

APPENDIX: PSEUDOPOTENTIAL AND LAPW METHODS

The full-potential linearized augmented plane-wave method (LAPW) (Ref. 64) was applied to calculate formation enthalpies for Al_pCu_q compounds, while a plane-wave code for pseudopotentials (PP) was applied to calculate first principles total energies for Al_pZn_q. In both approaches the exchange correlation term was always treated by the local density approximation of Ceperley and Alder[65] in the parametrization of Perdew and Zunger.[66]

In the *plane-wave pseudopotential calculation*, the kinetic energy and the implementation of Kleinman-Bylander[67] nonlocal potentials are performed in reciprocal space, the local potential and exchange correlation energy are calculated in real space. For a given occupied screened potential, the occupied eigenstates at different k points are calculated using the conjugate gradient method. The conjugate gradient line minimization is performed one state at a time. Since the input potential is fixed during the conjugate gradient process, analytic energy curves can be used to determine the energy minimum in the line minimization. At any given time, only the wave functions of one k point need to be stored in the memory, while all other wave functions are stored on disk. This method allows calculations with a large number of k points as required in our study. As in the conventional approach,[68] an outside loop is provided to converge the self-consistent field. While Kerker's approach[73] is used to mix the input and output screened potential differently at different reciprocal vector components, Pulay's algorithm[74] is used to take advantage of all the previous input-output potential pairs to determine the optimal input potential for the next iteration.

The atomic pseudopotentials (PP) were generated using the scheme of Troullier and Martins[69] whereby $3d$ electrons of Cu and Zn were treated as valence electrons. The cutoff radii used for s, p, and d pseudopotentials are $r_s(\mathrm{Al}) = 2.2$ Å, $r_p(\mathrm{Al}) = 2.0$ Å, $r_s(\mathrm{Cu}) = 1.8$ Å, $r_p(\mathrm{Cu}) = 2.3$ Å, $r_d(\mathrm{Cu}) = 1.5$ Å, $r_s(\mathrm{Zn}) = 2.0$ Å, $r_p(\mathrm{Zn}) = 2.6$ Å, $r_d(\mathrm{Zn}) = 2.0$ Å. Atomic PP and all-electron eigenvalues agree for all elements better than 0.07 meV. To guarantee stability of the PP a number of transferability tests were made, e.g., excitation energies were calculated. Furthermore, the chosen non-local Kleinman-Bylander-form[67] of the pseudopotentials demands a ''ghost-state'' analysis by Gonze *et al.*[70] to find out if there are unphysical bound states or resonances in the valence spectrum of the atom. In all cases the selection of s- as local potential does not lead to any ''ghost states.''

TABLE VII. Calculated values of lattice parameters a and bulk moduli $B0$ for fcc-Zn, Al, and Cu using the LAPW as well as the pseudopotenital method and comparison to experimental values.

Element	Cu	Al	fcc-Zn
$a_{\mathrm{eq}}^{\mathrm{exp}}$ [Å]	3.61	4.03	
$a_{\mathrm{eq}}^{\mathrm{PP}}$ [Å]	3.56	3.96	3.82
$a_{\mathrm{eq}}^{\mathrm{LAPW}}$ [Å]	3.53	3.98	3.79
B_0^{exp} [MBar]	1.37	0.72	
B_0^{PP} [MBar]	1.78	0.84	0.98
B_0^{LAPW} [MBar]	1.98	0.84	1.12

For the LAPW calculations, we have used the code of Wei and Krakauer.[64] The Perdew-Zunger[66] parametrization of the Ceperley-Alder[65] exchange correlation functional was used, along with a highly converged basis set corresponding to $E_{\mathrm{cut}} = 16.7$ Ry ($RK_{\max} = 9$). Other parameters were: a charge density cutoff of $RK_{\max} = 20$, muffin-tin radii of $R_{\mathrm{Al}} = 2.4$ and $R_{\mathrm{Cu}} = 2.2$ a.u., the maximum difference in the angular momenta in the nonspherical Hamiltonian terms of $l_{\max} = 4$, and the maximum angular momenta in the nonspherical charge densities and potentials inside the muffin-tin spheres of $l_{\max} = 8$. Equivalent k points corresponding to an $8 \times 8 \times 8$ mesh (or larger) were used[51] for Al-Cu compounds.

For the plane-wave basis a cutoff energy of 80 Ry is necessary in order to guarantee convergence of the calculations. Total energy calculations for fcc-Zn, Al, Cu by use of LAPW and the pseudopotential plane-wave-code give nearly the same lattice parameters a and bulk moduli B_0 for both methods. The values are given in Table VII, experimental values are taken from Ref. 71 (for hypothetical fcc Zn there are no experimental data).

Moreover, the spectra of eigenvalues at the Γ, L, and X point were compared between LAPW and pseudopotentials results for fcc-Zn, Cu, and Al. In all cases the deviation between differences of eigenvalues are smaller than 60 meV. In a last test formation enthalpies for a number of Al_pZn_q compounds were calculated using both methods. As an example we give the enthalpy for $V2$ [Al_2Zn_2 in (111)] which belongs to the structures with an extremely small formation enthalpy demanding an unusual large set of k points as discussed in Sec. III D. The values amount to $\Delta H_f^{\mathrm{LAPW}}(V2) = +3.6$ meV and $\Delta H_f^{\mathrm{PP}}(V2) = +4.8$ meV using $16 \times 16 \times 16$ k points.

[1] J. E. Hatch, *Aluminum: Properties and Physical Metallurgy* (American Society for Metals, Metals Park, Ohio, 1998).

[2] J. Desplat, F. Bley, F. Livet, and O. Schaerpf, Acta Mater. **44**, 1849 (1996).

[3] D. R. Haeffner and J. B. Cohen, Acta Metall. **37**, 2185 (1989).

[4] J. Cahn, Acta Metall. **9**, 795 (1961); **10**, 179 (1962).

[5] D. de Fontaine, Solid State Phys. **34**, 73 (1979); Metall. Trans. A **12**, 559 (1981).

[6] H. Löffler, V. Synecek, M. Simerska, G. Wendrock, P. Bartuska, and R. Kroggel, Phys. Status Solidi A **65**, 197 (1981).

[7] J. L. Murray, Bull. Alloy Phase Diagrams **4**, 55 (1983).

[8] E. Matsubara and J. B. Cohen, Acta Metall. **12**, 2129 (1983).

[9] C. R. Houska and B. L. Averbach, J. Appl. Phys. **30**, 1525 (1959).

[10] B. Borie and C. J. Sparks, Acta Crystallogr. **17**, 827 (1964).

[11] J. E. Epperson, P. Furnrohr, and C. Ortiz, Acta Crystallogr., Sect. A: Cryst. Phys., Diffr., Theor. Gen. Crystallogr. **34**, 667 (1978).

[12] B. Schoenfeld, H. Reolofs, A. Malik, G. Kostorz, J. Plessing, and H. Neuhauser, Acta Matter. **44**, 335 (1996).
[13] R. Hultgren, P. D. Desai, D. T. Hawkins, M. Gleiser, and K. K. Kelley, *Selected Values of the Thermodynamic Properties of Binary Alloys* (American Society for Metals, Metals Park, Ohio, 1973).
[14] M. Hansen, *Consitution of Binary Alloys* (McGraw-Hill, New York, 1958).
[15] T. B. Massalski, *Binary Alloy Phase Diagram*, edited by J. L. Murray, L. H. Bennett, and H. Baker (American Society for Metals, Metals Park, Ohio, 1986).
[16] D. B. Laks, L. G. Ferreira, S. Froyen, and A. Zunger, Phys. Rev. B **46**, 12 587 (1992).
[17] A. Zunger, NATO ASI on *Statics and Dynamics of Alloy Phase Transformations*, edited by P. E. A. Turchi and A. Gonis (Plenum Press, New York, 1994), p. 361.
[18] M. Simerska, V. Synecek, and V. Sima, Czech. J. Phys., Sect. B **24**, 543 (1974).
[19] M. Simerska and B. Bartuska, Czech. J. Phys., Sect. B **24**, 654 (1974).
[20] D. Schwahn and W. Schmatz, Acta Metall. **26**, 1571 (1978).
[21] J. B. Cohen, Solid State Phys. **39**, 131 (1986).
[22] J. Deguercy, M. F. Denanot, M. Fumeron, J. P. Guillot, and J. Caisso, Acta Metall. **30**, 1921 (1982).
[23] R. Ramlau and H. Löffler, Phys. Status Solidi A **79**, 141 (1983).
[24] G. Hübner, H. Löffler, and G. Wendrock, Cryst. Res. Technol. **21**, 8 (1986).
[25] V. Gerold, W. Siebke, and G. Tempus, Phys. Status Solidi A **104**, 213 (1987).
[26] A. Guilarducci de Salva, J. P. Simon, F. Livet, and P. Guyot, Scr. Metall. **21**, 1061 (1987).
[27] A. Guinier, Solid State Phys. **9**, 293 (1959).
[28] For a review of the controversial results on coherent precipitation in Al-Cu, see V. Gerold, Scr. Metall. **22**, 927 (1988).
[29] C. Wolverton, Philos. Mag. Lett. **79**, 683 (1999).
[30] Z. W. Lu, S.-H. Wei, and A. Zunger, Phys. Rev. B **41**, 2699 (1990).
[31] J. M. Wills, O. Eriksson, P. Söderlind, and A. M. Boring, Phys. Rev. Lett. **68**, 2802 (1992).
[32] T. Kraft, P. M. Marcus, M. Methfessel, and M. Scheffler, Phys. Rev. B **48**, 5886 (1993).
[33] P. J. Craievich, M. Weinert, J. M. Sanchez, and R. E. Watson, Phys. Rev. Lett. **72**, 3076 (1994).
[34] P. Alippi, P. M. Marcus, and M. Scheffler, Phys. Rev. Lett. **78**, 3892 (1997).
[35] M. Sob, L. G. Wang, and V. Vitek, Comput. Mater. Sci. **8**, 100 (1997).
[36] D. Singh and D. A. Papaconstantopoulos, Phys. Rev. B **42**, 8885 (1990).
[37] J. X. Zheng-Johansson, O. Eriksson, and B. Johansson, Phys. Rev. B **59**, 6131 (1999).
[38] A. Zunger, in *Handbook of Crystal Growth*, edited by T. D. J. Hurle (Elsevier, Amsterdam, 1994), Vol. 3, p. 997, and references therein.
[39] D. M. Wood and A. Zunger, Phys. Rev. Lett. **61**, 1501 (1988).
[40] D. J. Bottomeley and P. Fons, J. Cryst. Growth **44**, 513 (1978).
[41] There are no negative values for the constituent strain energy in Fig. 3. This is due to the following: In the minimization of Eq. (2), we have restricted the lattice constant range of a_p to be between a_{Al} and a_{Zn} (the lattice constant of undistorted fcc Zn). Relaxing this constraint only affects the constituent strain for Zn-rich compositions and thus does not affect the results of this paper.
[42] V. Ozoliņš, C. Wolverton, and A. Zunger, Phys. Rev. B **57**, 4816 (1998).
[43] V. Ozoliņš, C. Wolverton, and A. Zunger, Phys. Rev. B **57**, 6427 (1998).
[44] C. Wolverton, V. Ozoliņš, and A. Zunger, Phys. Rev. B **57**, 4332 (1998).
[45] Recently, it has been found [C. Wolverton, V. Ozoliņš, and A. Zunger (unpublished)] that attenuating the constituent strain term can be important in strongly anharmonic, ordering type systems. Attenuating the constituent strain does not have any significant effect on the Al-rich Al-Cu and Al-Zn systems considered in this paper.
[46] Z. W. Lu, D. B. Laks, S.-H. Wei, and A. Zunger, Phys. Rev. B **50**, 6642 (1994).
[47] C. Wolverton and A. Zunger, Phys. Rev. Lett. **75**, 3162 (1995).
[48] A. Silverman, A. Zunger, R. Kalish, and J. Adler, J. Phys.: Condens. Matter **7**, 1167 (1995).
[49] D. J. Chadi and M. L. Cohen, Phys. Rev. B **8**, 5747 (1973).
[50] H. J. Monkhorst and J. D. Pack, Phys. Rev. B **13**, 5188 (1976).
[51] S. Froyen, Phys. Rev. B **39**, 3168 (1989).
[52] G. D. Garbulsky and G. Ceder, Phys. Rev. B **51**, 67 (1995).
[53] S. an Mey, Z. Metallkd. **84**, 451 (1993).
[54] H. L. Lukas, E.-Th. Henig, and B. Zimmermann, Calphad **I**, 225 (1977).
[55] F. E. Wittig and L. Schöffl, Z. Metallkd. **51**, 700 (1960).
[56] R. A. Connel and D. B. Downie, Met. Sci. **7**, 12 (1973).
[57] J. E. Hilliard, B. L. Averbach, and M. Cohen, Acta Metall. **2**, 621 (1954).
[58] J. Hair and D. B. Downie, Faraday Symp. Chem. Soc. **8**, 56 (1973).
[59] W. Oelsen and W. Middel, Mitt. K.-Wilh.-Inst. Eisenforsch **19**, 1 (1937).
[60] A reference to J. Murray, private communication is given for the experimental heat of solution for Cu in Al in C. Lane Rohrer, Modell. Simul. Mater. Sci. Eng. **2**, 119 (1994).
[61] F. E. Wittig and G. Keil, Z. Metallkd. **54**, 576 (1963).
[62] M. A. Krivoglaz, *Diffuse Scattering of X-rays and Neutrons by Fluctuations* (Springer, New York, 1996).
[63] L. H. Schwartz and J. B. Cohen, *Diffraction from Materials* (Academic Press, New York, 1977).
[64] S.-H. Wei and H. Krakauer, Phys. Rev. Lett. **55**, 1200 (1985); D. J. Singh, *Planewaves, Pseudopotentials and the LAPW Method* (Kluwer, Boston, 1994).
[65] D. M. Ceperley and B. J. Alder, Phys. Rev. Lett. **45**, 566 (1980).
[66] J. P. Perdew and A. Zunger, Phys. Rev. B **23**, 5048 (1981).
[67] L. Kleinman and D. M. Bylander, Phys. Rev. Lett. **48**, 1425 (1982).
[68] M. C. Payne, M. P. Feter, D. C. Allan, T. A. Arias, and J. D. Joannopoulos, Rev. Mod. Phys. **64**, 1045 (1992).
[69] N. Troullier and J. L. Martins, Phys. Rev. B **43**, 1993 (1991).
[70] X. Gonze, R. Stumpf, and M. Scheffler, Phys. Rev. B **44**, 8503 (1991).
[71] C. Kittel, *Solid State Physics* (Wiley, New York 1976).
[72] P. P. Müller, B. Schoenfeld, G. Kostorz, and W. Buhrer, Acta Metall. **37**, 2125 (1989).
[73] G. P. Kerker, Phys. Rev. B **23**, 3082 (1981).
[74] P. Pulay, Chem. Phys. Lett. **73**, 393 (1980).
[75] J. L. Murray, Int. Met. Rev. **30**, 211 (1985).